



Unravelling the structural and chemical features influencing deformation-induced martensitic transformations in steels

G.K. Tirumalasetty,^{a,b,*} M.A. van Huis,^{b,c} C. Kwakernaak,^d J. Sietsma,^d W.G. Sloof^d and H.W. Zandbergen^{b,*}

^aMaterials innovation institute (M2i), Mekelweg 2, 2628 CD Delft, The Netherlands

^bKavli Institute of Nanoscience, Delft University of Technology, Lorentzweg 1, 2628 CJ Delft, The Netherlands

^cSoft Condensed Matter, Debye Institute for Nanomaterials Science, Utrecht University, Princetonplein 5, 3584 CC Utrecht, The Netherlands

^dDepartment of Materials Science and Engineering, Delft University of Technology, Mekelweg 2, 2628 CD Delft, The Netherlands

Received 25 August 2013; revised 27 September 2013; accepted 28 September 2013

Available online 3 October 2013

A combination of electron backscattered diffraction and high-sensitivity electron probe microanalysis was used to correlate the changes in microstructural features upon deformation with local chemical composition in transformation-induced plasticity steels. A novel cleaning procedure was developed that allows complete monitoring of transformation and deformation processes in relation to the local crystal structure, microstructure and chemical composition. Here we show direct evidence that local variations in manganese content enable a gradual transformation of the retained austenite grains.

© 2013 Acta Materialia Inc. Published by Elsevier Ltd. All rights reserved.

Keywords: Transformation-induced plasticity (TRIP) steel; Electron backscattered diffraction (EBSD); Electron probe microanalysis (EPMA); Chemical mapping; Martensitic transformation

The intriguing phenomenon of martensitic (diffusionless) phase transformations occurring during deformation was recognized by Sauveur [1] in 1924 by means of his torsion tests on iron bars. Surprisingly, it led to a substantial increase in ductility, and the effect was later termed transformation-induced plasticity (TRIP) [2]. The first practical exploitation of the TRIP effect came in 1967 from Zackay and co-workers, who developed steels with dramatically improved elongation as a consequence of the deformation-induced martensitic transformation [3]. Considerable scientific and technological interest grew in the early 1970s in the field of zirconia-containing ceramics exhibiting such phase transformations [4]. The concept of deformation-induced phase transformation has also been applied to polymers [5] and brittle bulk metallic glasses [6], and very recently to titanium-based biomedical alloys [7].

In view of the technological importance, there is a strong interest in understanding deformation-induced phase transformations, in particular to assess the role of various microstructural parameters such as the local chemical composition [8], grain size [9], crystal lattice orientation in relation to strain direction [10] and the location of the grain in relation to its surrounding grains [11]. An accurate understanding of all these factors and their interplay will allow fine tuning of phase transformations resulting in an enhanced control over the material properties [12].

Despite the fact that steels are amongst the most extensively investigated materials, many features of the martensitic transformation process during deformation remain unclarified to date. In particular, the role of alloying elements such as C, Mn, Si and Al during transformations is poorly understood [13] and there is an increasing need to gain fundamental insights into this topic. In this study, two steels, with chemical compositions of (wt.%) Fe–1.65Mn–1.53Si–0.037Al–0.199C (Si-alloyed TRIP steel) [11] and Fe–1.62Mn–0.35Si–0.91Al–0.187C (Al-alloyed TRIP steel) [14], are investigated. Both of these steels are commercially produced on an industrial

* Corresponding authors at: Kavli Institute of Nanoscience, Delft University of Technology, Lorentzweg 1, 2628 CJ Delft, The Netherlands. Tel.: +31 15 2781536; fax: +31 15 2786600 (G.K. Tirumalasetty); e-mail: ganeshkumar.india@gmail.com

hot dip galvanizing line using a conventional intercritical annealing cycle followed by cooling to around 400–460 °C, isothermal holding at this temperature and finally cooling to room temperature.

In order to obtain combined information of the crystallographic structure, orientation and chemical composition of each grain in relation to its neighbouring grains, and their changes upon an overall deformation and the strain direction, we have used a combination of two techniques: electron backscattered diffraction (EBSD) and electron probe microanalysis (EPMA). EBSD enables to monitor the microstructural changes of individual grains during deformation. For instance, we recently reported an EBSD study showing that metastable austenite grains rotate within the matrix (of ferrite) during the tensile tests in TRIP steels [11], thereby contributing to the high ductility of these steels. EPMA is a very reliable analytical technique to measure the chemical composition. Although EBSD and EPMA can provide the required information, their actual application for monitoring phase transformations is hampered by an inevitable formation of carbon contamination on the surface. This carbon layer is deposited during the measurements due to the decomposition of residual hydrocarbon gases [15] by the electron beam, which deteriorates the quality of the EBSD data and makes the EPMA carbon content analysis totally unreliable.

It is thus essential to remove the contamination formed during each EBSD and EPMA measurement prior to additional EBSD or EPMA experiments performed after straining. For this purpose, we have successfully developed a two-step plasma cleaning procedure, using a very low-energy oxygen plasma followed by a hydrogen radicals plasma (details in the supporting information (SI)). The key component is the use of low-energy hydrogen radicals, which can only result in chemical processes at the surface [16], instead of the generally used physical sputtering. We obtained excellent results using first oxygen plasma cleaning for 3 min followed by hydrogen plasma cleaning for 40 min. The EBSD data after cleaning showed the same quality as the EBSD data on the virgin surface: in both cases 85% of the EBSD patterns could be indexed, whereas with the carbon contamination layer only 10%

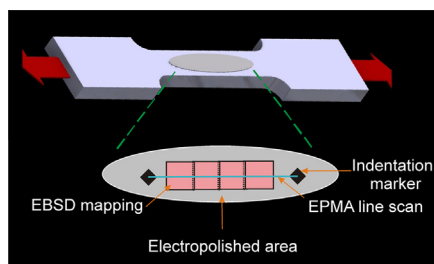


Figure 1. Schematic of a dog-bone-shaped TRIP steel sample subjected to tensile deformation. The inset shows the central electropolished area where adjacent EBSD maps and an EPMA line scan are recorded between markers. The indentation markers are also visible in the experimental SEM images (Fig. 2). Experimental details are given in the SI.

could be indexed and with oxygen plasma cleaning alone only 30% could be indexed.

A schematic of the sample and the EBSD and EMPA measurements is shown in Figure 1. Dog-bone-shaped samples were electropolished in order to have a surface layer that is not mechanically deformed. Markers were created by indentation with a Vickers indenter, and EBSD and EPMA mapping was performed between these markers. Scanning electron microscopy (SEM) images were recorded before and after EBSD measurements to track the respective locations as shown in Figure 2. The samples were plasma cleaned after each EBSD or EMPA analysis using the cleaning procedure described above. After the EBSD and EPMA measurements, the samples were deformed and EBSD maps were recorded again on the same area. The samples were only lightly strained to follow the first transformations during the deformation process. SEM–EBSD was performed using a JEOL JSM 6500F microscope operated at 20 kV, and EPMA was performed using a JEOL JXA 8900R microprobe operated at 10 kV and 50 nA beam current with a spot size of 500 nm (more experimental details in SI).

Figures 3A and S2A show a typical TRIP steel microstructure consisting of ferrite matrix (coloured green) and metastable grains of retained austenite (coloured red). Retained austenite, which has a face-centred cubic structure, and ferrite, which has a body-centred cubic structure, can be easily distinguished by EBSD software because of their different crystallographic structures. Grains of martensite, grain boundaries and areas with a high dislocation density are not indexed by the EBSD software due to the poor quality of the Kikuchi patterns and are imaged in black in the phase identification maps. An EPMA line scan was performed on the EBSD mapped regions, as shown in Figures 3A and S2A, and the corresponding elemental compositions of the retained austenite grains are plotted in Figures 3C–E and S2C–E. Among all of the austenite grains intersected by the

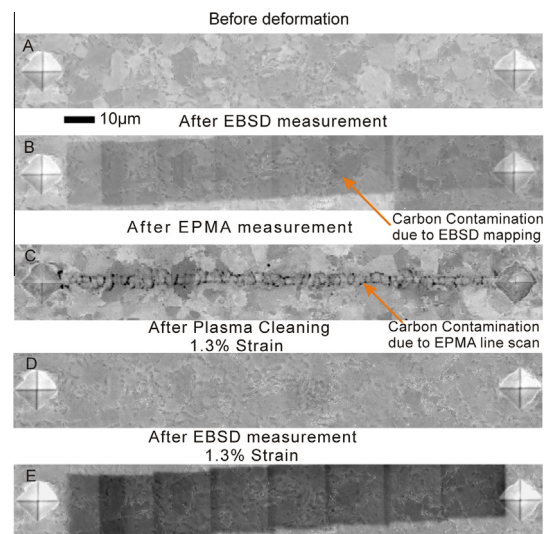


Figure 2. (A, B, D, E) SEM and (C) backscattered EPMA image of Al-alloyed TRIP steel indicating carbon contamination caused by EBSD mapping (B, E) and by the EPMA line scan (C). (D) Removal of carbon contamination by plasma cleaning.

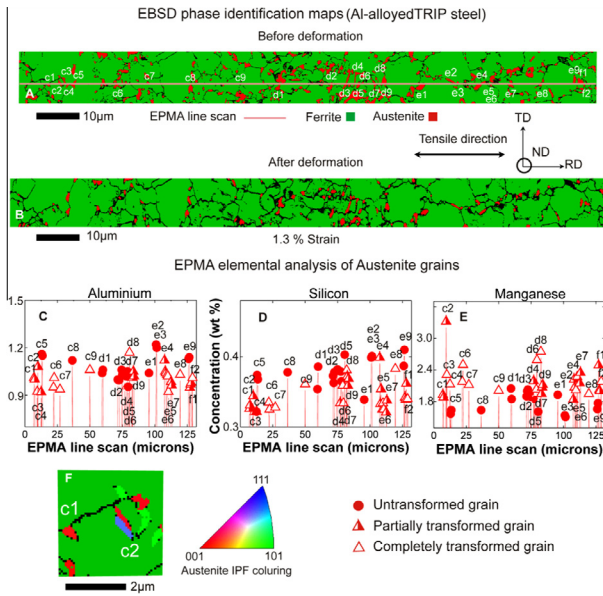


Figure 3. EBSD phase identification maps of Al-alloyed TRIP steel showing retained austenite grains labelled (c1–c9, d1–d9, e1–e9, f1, f2) (A) before and (B) after deformation and the EPMA composition profile of (C) aluminium, (D) silicon and (E) manganese corresponding to retained austenite grains. (F) Inverse pole figure map showing austenite grain C2 with a twin fault. The accuracies are given in Table S2 (SI).

EPMA line scan, it is clear from Figure S2B that grains a4-UT and a7-UT remain untransformed (UT), whereas grains a5-CT, a6-CT and a8-CT are completely transformed (CT) after deformation. Strikingly, the EPMA chemical composition maps in Figure S2C show that grains a4-UT and a7-UT contain very low manganese concentrations and grains a5-CT, a6-CT and a8-CT contain relatively very high Mn concentrations. Furthermore, Figure S2D shows that grains a4-UT and a7-UT contain fairly high silicon concentrations. This contradicts the existing experimental literature on steels [17,18], which suggests that lower Mn and higher Si contents should destabilize the austenite and lead to the early onset of martensitic transformation.

In the literature, several factors affecting the martensitic transformation are given: (i) the local carbon concentration in austenite [8]; (ii) the grain size of the austenite grains [9]; (iii) the crystallographic orientation of austenite grains with respect to the loading direction [10]; and (iv) the position of the austenite grains within the ferrite matrix [11]. These factors were also closely assessed for these grains with the help of EBSD and EPMA analysis. Regarding the effect of carbon concentration, the EPMA maps in Figure S2E clearly show that grain a4-UT has a very low carbon concentration, which should facilitate transformation. Regarding the grain size effect, grain a7-UT has a very large grain size, which should result in early transformation. Regarding the crystallographic effect, the Schmid factors (see SI) can be used to predict the ease of transformation based on the crystallographic orientation of a given grain to the strain direction. It is clear from Figure S3A and B that grains a4-UT and a7-UT exhibit different orienta-

tions, with a7-UT having a higher Schmid factor, which should promote easy slip and assist the transformation of this grain. Regarding the effect of the location of the austenite grain, grain a4-UT, which is located at the grain boundary, should facilitate an early transformation. In view of all the above observations, we conclude that both Mn and or Si majorly influence the transformation of the austenite grains in this steel.

Aluminium is another element that can influence the transformation behaviour [19]. The Si-alloyed TRIP steel shown in Figure S2 has a very low Al content, and therefore we investigated an Al-alloyed TRIP steel as well. The EBSD–EPMA results are displayed in Figure 3. As observed in panels C and D, the Al and Si contents do not have a major influence on the transformation. However, we find a consistent trend that austenite grains having higher Mn contents (Fig. 3E) transform earlier during the deformation process. The transformation behaviour of all the austenite grains and various parameters influencing the transformation are summarized in Table S1. We conclude that local Mn contents in austenite grains strongly influence the transformation in both TRIP steels.

The results clearly show that Mn-rich austenite grains transform earlier during the deformation process. As Mn stabilizes austenite [18], it cannot be a thermodynamic effect and must be kinematic in nature, thus local configurations must lower the energy barrier for the transformation. Possible reasons for the faster transformation of Mn-rich austenite grains are: (i) enhanced strain at the grain boundaries due to Mn segregation;

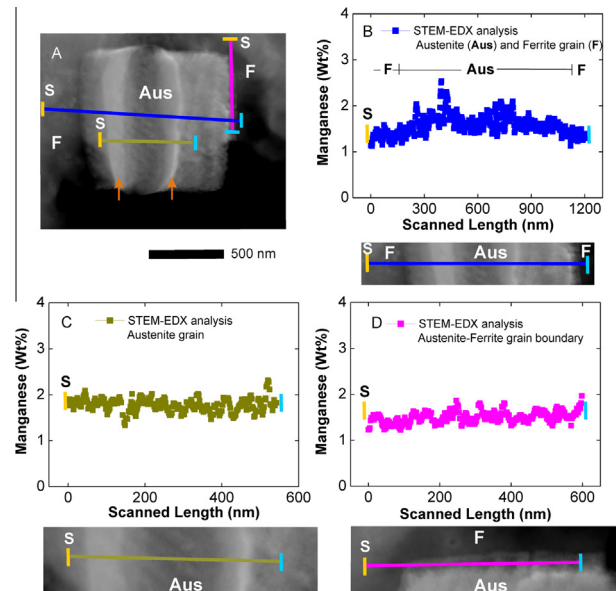


Figure 4. (A) TEM micrograph of Si-alloyed TRIP-assisted steel showing a twinned austenite grain (Aus) within the ferrite matrix (F). (B, C) STEM–EDX composition profile and corresponding TEM image of ferrite (B) and austenite (C) grains and the austenite–ferrite grain boundary (D). The gold marker (S) indicates the start and cyan marker (F) indicates the end point of the EDX line scans. Orange arrows indicate the position of twin boundaries. (For interpretation of the references to colour in this figure legend, the reader is referred to the web version of this article.)

(ii) internal additional stresses due to variations in Mn concentrations within the grain; or (iii) the twin boundaries that were observed in some (about 20%) of the Mn-rich austenite grains (Figs. S3–S5). In order to verify these issues, we performed a chemical analysis on a twinned austenite grain using energy-dispersive X-ray spectrometry (EDX) within a Tecnai 20F transmission electron microscope (TEM) operated at 200 kV (details in SI). The results are shown in Figure 4. Our analysis shows no Mn enrichment at the austenite–ferrite grain boundary or at the twin boundaries of austenite grains. However, a clear inhomogeneous distribution of Mn (with local variations in concentration up to 40–50%) was observed within the twinned austenite grain. The variation in Mn content is also consistent with the EPMA concentration maps (Fig. S2) of some of the transformed grains without twin faults. We propose that Mn variations within the austenite grain cause the early martensitic nucleation. At a very local scale, substitution of Fe by Mn leads to a lattice increase [20], which can result in local strain acting as a trigger for transformation. Once started, the transformation proceeds at high speed (~2 times the speed of sound) [17], resulting in a full transformation to martensite.

Experimental studies [21] indicate that the retained austenite grains should transform at different moments in time (in the limit of one by one) during the tensile deformation, thereby delaying the onset of necking and microcrack initiation, leading to extended ductility in these materials. Here we show that, by variation of the manganese concentration, in combination with microstructural parameters such as grain size, orientations and positioning of grains within the ferritic matrix, the occurrence of phase transformations can be “designed” such that they occur sequentially, which leads to desirable properties. Furthermore, our results show the need for detailed models, taking into account not only the thermodynamics but also the kinetics, whereby the effects of local variations in concentration on the scales of 100 nm as well as several microns should be included, as well as modelling for the optimum size and shape of the grains. From a technological and scientific perspective, these results call for a revisit of the systems studied, in particular by examining the local composition, because there is a strong interrelation between the local composition, the microstructure and mechanical properties.

This research was funded by the Materials innovation institute M2i (project No. MC5.06280a). The authors thank F.T. Molkenboer, N.B. Koster (TNO) and G. Schneider for plasma cleaning, S.R.K. Malladi and M. Neklyudova for STEM-EDX, and N.H. van Dijk, S. Turteltaub and B.J. Thijsse (DUT) for useful discussions. We thank Dr. D.N. Hanlon (Tata Steel RDT) for providing sample material and constructive discussions.

Supplementary data associated with this article can be found, in the online version, at <http://dx.doi.org/10.1016/j.scriptamat.2013.09.027>.

- [1] A. Sauveur, *Iron Age* 113 (1924) 581.
- [2] M. De Jong, G.W. Rathenau, *Nature* 181 (1958) 1396–1397.
- [3] V.F. Zackay, E.R. Parker, D. Fahr, R. Bush, *Trans. ASM* 60 (1967) 252–259.
- [4] R.C. Garvie, R.T. Pascoe, R.H.J. Hannink, *Nature* 258 (1975) 703–705.
- [5] F. Auremma, C. De Rosa, S. Esposito, G.R. Mitchell, *Angew. Chem.* 46 (2007) 4325–4328.
- [6] Y. Wu, Y.H. Xiao, G.L. Chen, C.T. Liu, Z.P. Lu, *Adv Mater.* 22 (2010) 2770–2773.
- [7] Z. Xiaoli, N. Mitsuo, N. Masaaki, M. Goro, F. Tadashi, *Acta Biomater.* 7 (2011) 3230–3236.
- [8] N.H. Van Dijk et al., *Acta Mater.* 53 (2005) 5439–5447.
- [9] E. Jimenez-Melero, N.H. van Dijk, L. Zhao, J. Sietsma, S.E. Offerman, J.P. Wright, S. van der Zwaag, *Scripta Mater.* 56 (2007) 421–424.
- [10] S.O. Kruijver et al., *J. Phys. IV* 104 (2003) 499–502.
- [11] G.K. Tirumalasetty, M.A. van Huis, C. Kwakernaak, J. Sietsma, W.G. Sloof, H.W. Zandbergen, *Acta Mater.* 60 (2012) 1311–1321.
- [12] S.E. Offerman et al., *Science* 298 (2002) 1003–1005.
- [13] M.A. Militzer, *Science* 298 (2002) 975–976.
- [14] G.K. Tirumalasetty et al., *Acta Mater.* 60 (2012) 7160–7168.
- [15] A.V. Crewe, *Science* 154 (1966) 729–738.
- [16] N.B. Koster, J.C.J. van der Donck, J.K. Stortelder, A.J. de Jong, F.T. Molkenboer *Proc. SPIE* 8322 (2012) 83220R.
- [17] N. Nishiyama, *Martensitic Transformation*, Academic Press, New York, 1978.
- [18] W.F. Smith, *Structure and Properties of Engineering Alloys*, McGraw-Hill, New York, 1993.
- [19] B.C. De Cooman, *Curr. Opin. Solid State Mater. Sci.* 8 (2004) 285–303.
- [20] A. Dick, T. Hickel, J. Neugebauer, *Steel Res. Int.* 80 (2009) 603–608.
- [21] H.C. Chen, H. Era, M. Shimizu, *Metall. Trans. A* 20A (1989) 437–445.